Journal of Materials Chemistry C

# Intensive Emission of Eu(III) β-Diketonate Complexes with Arsine Oxide Ligands

| | |
|---|---|
| Journal: | *Journal of Materials Chemistry C* |
| Manuscript ID | TC-ART-09-2023-003297.R1 |
| Article Type: | Paper |
| Date Submitted by the Author: | 25-Oct-2023 |
| Complete List of Authors: | Shimoji, Haruki; Kyoto Institute of Technology, Faculty of Molecular Chemistry and Engineering<br>Fujii, Toshiki; Kyoto Institute of Technology, Graduate School of Science and Technology<br>Sumida, Akifumi; Kyoto Institute of Technology, Faculty of Molecular Chemistry and Engineering<br>Kitagawa, Yuichi; Hokkaido University, Faculty of Engineering<br>Hasegawa, Yasuchika; Hokkaido University, Faculty of Engineering<br>Imoto, Hiroaki; Kyoto Institute of Technology, Faculty of Molecular Chemistry and Engineering<br>Naka, Kensuke; Kyoto Institute of Technology, Department of Chemistry and Materials Technology |
| | |

ARTICLE

# Intensive Emission of Eu(III) β-Diketonate Complexes with Arsine Oxide Ligands

Received 00th January 20xx,
Accepted 00th January 20xx

DOI: 10.1039/x0xx00000x

Haruki Shimoji,[a] Toshiki Fujii,[a] Akifumi Sumida,[a] Yuichi Kitagawa,[bc] Yasuchika Hasegawa,[bc] Hiroaki Imoto,*[ad] Kensuke Naka*[ae]

The development of luminescent lanthanide complexes hinges significantly on the judicious combination of counter anions and neutral ligands. The hexafluoroacetylacetonate (hfa) anion is a typical example of the counter anions used in this application because its low-vibrational C–F bonds are beneficial in restricting non-radiative deactivation. Recently, arsine oxide has emerged as a promising alternative to phosphine oxide, which is a neutral ligand typically utilized in luminescent lanthanide complexes. However, the use of arsine oxide has been limited to experiments involving europium trinitrate ($Eu(NO_3)_3$). This study synthesized $Eu^{3+}$ complexes incorporating arsine oxide and hfa ligands, and investigated their photophysical properties. The results demonstrated that the use of the tri(1-naphtyl)arsine oxide ligand led to a highly efficient red emission. Fascinatingly, the $Eu^{3+}$ complex with tri(1-naphthyl)arsine oxide exhibited luminescence even at 500 K, in contrast to other complexes whose luminescence ceased at this elevated temperature.

## Introduction

Lanthanide (Ln) complexes, which employ lanthanide ions ($Ln^{3+}$) as the luminescent core, are garnering significant attention in the fields of electronics and bio-imaging. $Ln^{3+}$ showcases unique luminescence stemming from 4f-4f electron transition.[1] Enclosed by the outer closed-shell 5s and 5p orbitals, the 4f orbitals of $Ln^{3+}$ remain relatively unaffected by external environmental factors. As a result, $Ln^{3+}$ complexes produce emissions that are nearly identical in wavelength to $Ln^{3+}$ alone, with an extremely narrow full width at half maximum (FWHM) values smaller than 10 nm. Given the difficulty of achieving such high color purity with organic dyes, where the FWHM often exceeds 50 nm, luminescent $Ln^{3+}$ complexes are increasingly used in laser oscillation and high-intensity LEDs. The demands of these photonic applications necessitate highly emissive $Ln^{3+}$ complexes.

However, the Laporte prohibition forbids 4f-4f transitions of $Ln^{3+}$, resulting in an exceptionally low molar absorptivity and thus a substantially low luminescence intensity. This limitation can be overcome with the use of antenna ligands.[2] The luminescence intensity of $Ln^{3+}$ can be significantly enhanced by transferring the excitation energy from high molar absorptivity antenna ligands to the $Ln^{3+}$ core. Consequently, active research is ongoing to design efficient antenna ligands to optimize the performances of lanthanide complexes.

Generally, enhancing the radiative rate constant ($k_r$) and reducing the non-radiative rate constant ($k_{nr}$) are crucial considerations in the molecular design of antenna ligands for highly emissive $Ln^{3+}$ complexes. First, the Laporte prohibition of the 4f-4f transition can be alleviated by lowering the symmetry around the $Ln^{3+}$ center, leading to an increase in $k_r$ through the promotion of electron dipole transition.[3] Second, the introduction of low-vibration bonds into the ligands can decrease $k_{nr}$ by suppressing the vibrational deactivation of excitons.[4] Given these principles, phosphine oxide is deemed to be a suitable neutral ligand. Its oxygen atom strongly coordinates to the $Eu^{3+}$ center, the P=O bond exhibits low vibration (approximately 1150–1160 $cm^{-1}$), and the molecular structure can be easily adapted to attain low symmetry.[5] These unique characteristics have spurred the development of luminescent $Ln^{3+}$ complexes with phosphine oxides.

In recent research, we demonstrated that an $Eu^{3+}$ complex with triphenylarsine oxide displayed superior ligand-to-metal energy transfer efficiency compared to its corresponding phosphine oxide analog, triphenylphosphine oxide.[6] We also studied the use of annulated arsine oxide ligands for luminescent $Eu^{3+}$ complexes and established a correlation between the ligand structure and photophysical properties of the ensuing $Eu^{3+}$ complexes.[7]

In these investigations involving arsine oxide ligands, nitrate anion ($NO_3^-$) served as the counter anion for the $Eu^{3+}$ cation. Because $NO_3^-$ does not significantly impact the energy transfer between the arsine oxide ligand and $Eu^{3+}$ core, it is an optimal

[a] Faculty of Molecular Chemistry and Engineering, Kyoto Institute of Technology, Goshokaido-cho, Matsugasaki, Sakyo-ku, Kyoto 606-8585, Japan. E-mail: himoto@kit.a.c.jp (HI), kenaka@kit.ac.jp (KN)
[b] Faculty of Engineering, Hokkaido University, Kita-ku, Sapporo, Hokkaido 606-8585, Japan.
[c] Institute for Chemical Reaction Design and Discovery (WPI-ICReDD), Hokkaido University, Sapporo, Hokkaido 001-0021, Japan.
[d] FOREST, JST, Honcho 4-1-8, Kawaguchi, Saitama 332-0012, Japan.
[e] Materials Innovation Lab, Kyoto Institute of Technology, Goshokaido-cho, Matsugasaki, Sakyo-ku, Kyoto 606-8585, Japan.

†Electronic Supplementary Information (ESI) available: FT-IR spectra, crystallographic data, structural analysis, photophysical and thermal properties, and computational calculations. See DOI: 10.1039/x0xx00000x

choice for studying the photophysical characteristics of arsine oxide ligands. However, the counter anion must be altered to achieve highly emissive $Eu^{3+}$ complexes. Hexafluoroacetylacetonate (hfa), which has a rigid bidentate structure and low-vibrational C–F bonds, is a suitable candidate that could assist in achieving a high photosensitization efficiency.[8] In this study, we synthesized new $Eu(hfa)_3(\mathbf{L})_2$ complexes (**L** = arsine oxide) and examined their structures and photophysical properties both experimentally and computationally (Figure 1).

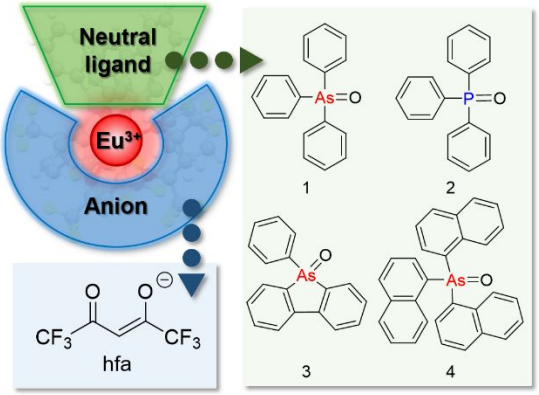


**Fig. 1** Molecular design of the luminescent $Eu^{3+}$ complexes examined in this work.

## Results and discussion

$Eu(hfa)_3$ and $Gd(hfa)_3$ complexes were prepared as shown in Scheme 1; the Gd complexes were also synthesized in order to analyze the photophysical properties of the corresponding Eu complexes as shown below. Triphenylarsine oxide (**1**) and triphenylphosphine oxide (**2**) were used to synthesize $Eu(hfa)_3(\mathbf{L})_2$ (**L** = **1** (**1-a**), **2** (**2-a**)) and $Gd(hfa)_3(\mathbf{L})_2$ (**L** = **1** (**1-b**), **2** (**2-b**)) to elucidate the differences between arsenic and phosphorus in relation to the structure and photophysical properties. In addition, 9-phenyl-9-arsafluorene oxide (**3**) and tri(1-naphtyl)arsine oxide (**4**) were selected to tune the electronic properties of the arsine oxide ligands, and $Eu(hfa)_3(\mathbf{L})_2$ (**L** = **3** (**3-a**), **4** (**4-a**)) and $Gd(hfa)_3(\mathbf{L})_2$ (**L** = **3** (**3-b**), **4** (**4-b**)) were synthesized. The products were purified by recrystallization from dichloromethane ($CH_2Cl_2$)/*n*-hexane. The structures of the complexes were determined by single crystal X-ray diffraction (SC-XRD) analyses, the high-resolution mass spectra, and the FT-IR spectra. After storage of the Eu complexes for more than a year under ambient condition in the solid states, no decomposition was observed, suggesting that they are sufficiently stable.

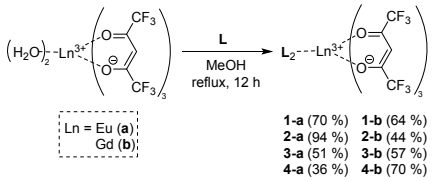


**Scheme 1.** Synthesis of $Eu^{3+}$ and $Gd^{3+}$ complexes.

The IR spectra of the $Eu^{3+}$ complexes showed negligible differences in the stretching vibrations of the C=O bonds of hfa (**1-a**, **2-a**, **3-a**: 1655 $cm^{-1}$, **4-a**: 1656 $cm^{-1}$), which implied that the arsine oxide or phosphine oxide ligands did not affect the electronic properties of hfa. It was also found that the As=O bonds showed low-vibration stretching (**1-a**: 892 $cm^{-1}$, **3-a**: 868 $cm^{-1}$, **4-a**: 864 $cm^{-1}$), even though the energies were slightly lower than that of the P=O bond (**2-a**: 1119 $cm^{-1}$). These low-vibrational bonds would assist in a highly efficient emission because $k_{nr}$ would be decreased by the restriction of the non-radiative vibrational deactivation.

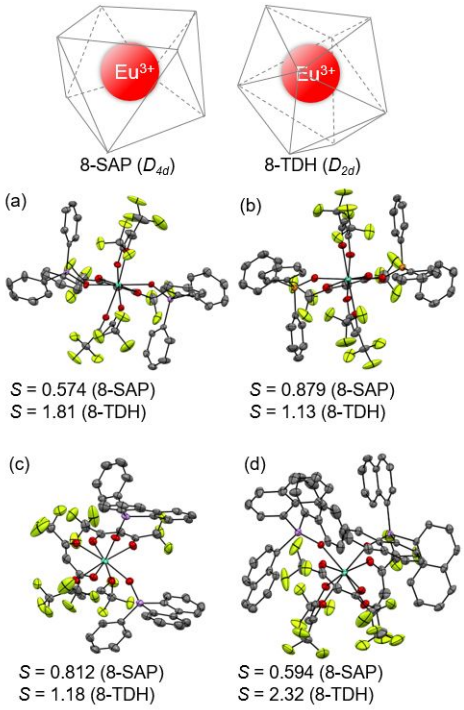


**Fig. 2** ORTEPs (50% probability for thermal ellipsoids) of (a) **1-a**, (b) **2-a**, (c) **3-a**, and (d) **4-a**. Hydrogen atoms and disordered atoms are omitted for clarity. The *S* values for 8-SAP and 8-TDH are shown.

The SC-XRD analyses revealed that the $Ln^{3+}$ centers of all the complexes had two neutral ligands (arsine oxide or phosphine oxide) and three hfa anions, resulting in 8-coordination structures (Tables S5–S12). The degree of distortion of the coordination structure was evaluated using continuous shape measurements on the first coordination sphere of each of the $Ln^{3+}$ complexes.[9] The measurements estimated shape value *S*, which is given by Equation (1):

$$S = \min[(\Sigma_{k=1}^{N}|Q_K - P_K|^2)/\Sigma_{k=1}^{N}|Q_K - Q_o|^2]\times 100, \quad (1)$$

where *N*, $Q_0$, $Q_k$, and $P_k$ are the number of vertices, center of mass of the actual structure, vertices of the actual structure, and vertices of the ideal structure, respectively. A lower *S* value indicated greater symmetry for the coordination structure. The coordination structure that gave the smallest *S* value among the various structures was adopted. The calculations (Figure 2) showed that all the $Eu^{3+}$ complexes had distorted 8-

coordination square antiprism (8-SAP, $D_{4d}$) geometric structures. The geometries of the $Gd^{3+}$ complexes were in good agreement with those of the corresponding $Eu^{3+}$ complexes (Table S13). Given the structures of **1-a** and **2-a**, the Eu···O=As distances (2.283(2) and 2.293(2) Å) were shorter than those of Eu···O=P (2.307(3) and 2.308(3) Å). This was probably because arsenic has a lower electronegativity than phosphorus, which resulted in a relatively larger polarization of the O=As bond, leading to stronger coordination bonding with the $Eu^{3+}$ center. Interestingly, steric repulsion occurred between the bulky 1-naphthyl groups, causing the coordination structure of **4-a** to be locally distorted, which was different from the typical 8-SAP geometry (Figure S4).

Previously, Hasegawa (one of the authors of this paper) et al., suggested that the dipole moment of antenna ligands may be related to the formation of coordination geometric structures in $Ln^{3+}$ complexes, and it was reported that an $Eu^{3+}$ complex with a ligand having a high dipole moment formed an 8-coordination trigonal dodecahedron (8-TDH, $D_{2d}$) structure.[10] The present study also used time-dependent density functional theory (TD-DFT) calculations based on the single-crystal X-ray structure analysis results to estimate the dipole moment parameters of each antenna ligand (Table S19). In arsenic-containing complexes **1-a**, **3-a**, and **4-a**, as the dipole moment increased, it became closer to the ideal 8-TDH geometry (Figure S19). This trend was consistent with results of the previous study by Hasegawa et al., and it was suggested that the dipole moment of the antenna ligand might be leading to the 8-TDH geometry even in the series of $Eu^{3+}$ complexes using arsine oxides.

The packing structures of the $Eu^{3+}$ complexes were compared because inter- and intramolecular interactions are important in emission efficiency. Molecular motions, which can cause non-radiative deactivation, can be suppressed by these interactions. The present $Eu^{3+}$ complexes formed CH/F interactions in the crystalline structures (Figures 3a and S3). In particular, there were more CH/F interactions in a crystal of **4-a** (11 CH/F interactions) than in the others (6 CH/F interactions). This observation will contribute to the inhibition of non-radiative deactivation (*vide infra*). Furthermore, a thermogravimetric analysis (TGA) was conducted to evaluate the thermal stability of the $Eu^{3+}$ complexes based on the temperature at which the sample lost 5 wt% of its original mass ($T_{d5}$) (Figure 3b, Table S18). The $T_{d5}$ value of **4-a** (284 °C) was significantly higher than those of the others (**1-a**: 240 °C, **2-a**: 247 °C, **3-a**: 244 °C). The relatively high stability of **4-a** is attributed to the robust molecular packing supported by inter- and intramolecular CH/F interactins, which was observed in the X-ray data. In addition, the thermal stability of the arsine oxide complexes was enhanced compared to that of $Eu(hfa)_3(H_2O)_2$, which indicated the stronger coordination of the arsine oxide ligands compared to that of the hydration water.

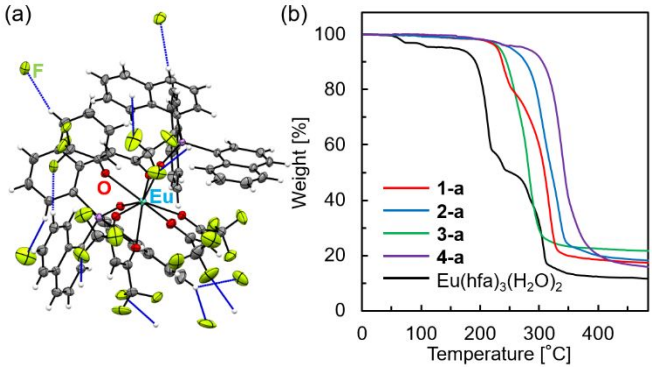


**Fig. 3** ORTEP of **4-a** (thermal ellipsoids: 50% probability level, with disordered atoms omitted for clarity). Blue lines indicate intra- and intermolecular CH/F interactions. (b) TGA thermograms of $Eu^{3+}$ complexes.

The photophysical properties of the $Eu^{3+}$ complexes were examined in the solid states (Table 1, Figures 4 and S15–S16). Prior to the PL measurements, it was confirmed that the powder XRD patterns of the bulk samples are in good agreement with those simulated by the SC-XRD data (Figure S18). The diffuse reflection spectra showed absorption maxima ($\lambda_{abs}$) at approximately 320 nm, which were attributed to the π-π* transition of the hfa ligand (Figure S6). The excitation maxima ($\lambda_{ex}$) were in agreement with the $\lambda_{abs}$ values, which implied that the excitation of the hfa ligand ($\lambda_{ex}$ = 347–350 nm) was necessary to achieve intensive emissions. The photoluminescence (PL) spectra of the $Eu^{3+}$ complexes showed peaks at 581, 593, 614, 653, and 702 nm, which were derived from the $^5D_0$-$^7F_J$ transitions ($J$ = 0, 1, 2, 3, and 4, respectively). The intensities of the f-f transition in the PL spectra were normalized at 593 nm, which was attributed to the magnetic dipole transition ($^5D_0$-$^7F_1$). In addition, the PL quantum yields were obtained through photosensitized energy transfer ($\Phi_{tot}$) and $Ln^{3+}$-center excitation ($\Phi_{f\text{-}f}$), and the photosensitized energy-transfer efficiencies were evaluated ($\eta_{sens} = \Phi_{tot}/\Phi_{f\text{-}f}$). The $\Phi_{f\text{-}f}$ and $\eta_{sens}$ values of **1-a** were higher than those of the previously reported $Eu(NO_3)_3$ complex of **1** with ethanol ($Eu(NO_3)_3$(**1**)$_2$(EtOH)).[6] In the case of the $NO_3^-$ complex, a solvent molecule such as EtOH coordinates to the $Eu^{3+}$ center to readily cause non-radiative deactivation. However, the bulky hfa ligands inhibited the coordination of such a solvent molecule, resulting in the avoidance of the non-radiative deactivation pathway. Furthermore, the $k_r$ values of the $Eu(hfa)_3$ complexes were significantly greater than those of the ethanol-free $Eu(NO_3)_3$ complexes (phenoxybenzene type) that we previously reported.[7] On the other hand, a slight increase in $k_{nr}$ was also observed as a result of vibrations caused by the C-H bonds of the hfa ligands.[8]

**Table 1.** Photophysical properties of $Eu^{3+}$ complexes at 298 K in the solid state.

| | $\lambda_{ex}$ [nm] | $I_{614}/I_{593}$[a,b] | $\tau_{obs}$[c,g] [ms] | $\Phi_{tot}$[d,g] [%] | $\Phi_{f\text{-}f}$[a,e,g] [%] | $k_r$[e] [$10^2 \cdot s^{-1}$] | $k_{nr}$[e] [$10^2 \cdot s^{-1}$] | $\eta_{sens}$[f] |
|---|---|---|---|---|---|---|---|---|
| **1-a** | 347 | 15.1 | 0.65 | 52 | 65 | 10.0 | 5.4 | 0.80 |
| $Eu(NO_3)_3$(**1**)$_2$(EtOH)[h] | 292 | 8.9 | 0.69 | 23 | 42 | 6.1 | 8.4 | 0.55 |
| **2-a** | 346 | 12.8 | 0.76 | 51 | 63 | 8.4 | 4.8 | 0.80 |
| **3-a** | 346 | 14.4 | 0.79 | 53 | 67 | 8.4 | 4.3 | 0.81 |
| **4-a** | 350 | 19.1 | 0.65 | 63 | 74 | 11.5 | 4.0 | 0.85 |

[a] Excited at 465 nm. [b] Relative intensity of $^5D_0 \rightarrow {}^7F_2$ transition (electric dipole) to $^5D_0 \rightarrow {}^7F_1$ (magnetic dipole). [c] Excitation at 340 nm (monitored at 614 nm). [d] Excited at $\lambda_{ex}$. [e] Calculated using equations 2–6 in the experimental section. $^5D_0 \rightarrow {}^7F_5$, and $^7F_6$ transitions were not considered in the calculation of the intrinsic quantum yields because the transition emission was very noisy owing to the weak emission intensity. [f] $\eta_{sens} = \Phi_{tot}/\Phi_{f\text{-}f}$. [g] It was confirmed that $\Phi_{tot}$, $\tau_{obs}$, and $\Phi_{f\text{-}f}$ were reproducible with errors within 1% in five measurements. [h] Cited from reference 6.

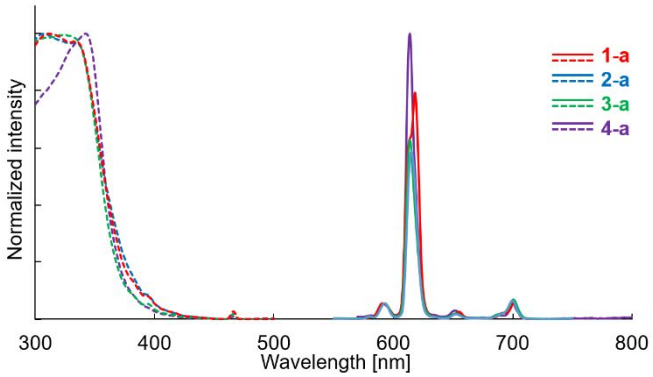


**Fig. 4** PL spectra (excitation wavelength $\lambda_{ex}$ = 465 nm, solid line) and excitation spectra (monitored wavelength $\lambda_{em}$ = 614 nm, dashed lines) of $Eu^{3+}$ complexes at 298 K in the solid state.

The results for **1-a** and **2-a** were compared in order to elucidate the influence of the pnictogen atom. The intensity ratio ($I_{ED}/I_{MD}$) of the emissions resulting from the electron dipole ($^5D_0$-$^7F_2$, $I_{ED}$ = intensity at 614 nm) and magnetic dipole ($^5D_0$-$^7F_1$, $I_{MD}$ = intensity at 593 nm) transitions of **1-a** ($I_{ED}/I_{MD}$ =15.1) was larger than that of **2-a** ($I_{ED}/I_{MD}$ = 12.8). In addition, the $k_r$ value of **1-a** (1000 $s^{-1}$) was slightly larger than that of **2-a** (840 $s^{-1}$). These results indicated that the f-f transition probability was enhanced by the arsenic atom. The higher polarizability of a ligand is known to lead to a higher f-f transition probability in static and dynamic coupling models; in particular, a relatively sensitive electron dipole transition tends to be promoted. The TD-DFT calculations revealed that **1-a** (5.08 debye) had a larger dipole moment than **2-a** (4.50 debye), which indicated that the electron dipole transition was enhanced by the dynamic coupling (Table S19). In contrast, a natural bond orbital (NBO) analysis demonstrated that there was negligible difference between **1-a** and **2-a** in relation to the charge of the oxygen atom of the pnictogen oxide ligand, and that static coupling hardly contributed to the difference in the efficiency of the electron dipole transition. This result was consistent with that reported in our previous work on $Eu(NO_3)_3$ complexes.[6] Thus, we concluded that arsine oxide is beneficial for luminescent $Eu^{3+}$ complexes with hfa ligands.

The $\Phi_{f\text{-}f}$ and $\eta_{sens}$ values of **3-a** were similar to those of **1-a**. In other words, the annulated structure of **3** had little influence on the photophysical properties of the $Eu(hfa)_3$ complex, although it was important in the $Eu(NO_3)_3$ complex.[7] In the case of the $Eu(NO_3)_3$ complex, the non-radiative deactivation due to molecular vibrations significantly diminished the emission efficiency, whereas the rigid chelating structure and low-vibrational C–F bonds of the hfa ligands made it possible to effectively avoid non-radiative deactivation. As a result, the influence of the rigidity of the arsine oxide ligands was minimized, and the difference between **1-a** and **3-a** in relation to the $\Phi_{f\text{-}f}$ and $\eta_{sens}$ values was negligible. Notably, **4-a** showed the highest $\Phi_{f\text{-}f}$, and significantly high $k_r$ and low $k_{nr}$ values were observed. As previously mentioned, the locally distorted primary coordination sphere of **4-a** contributed to the relaxation of Laporte's rule, leading to the increase in $k_r$. The low $k_{nr}$ value was due to the robust molecular packing in the crystalline state as observed in the X-ray data. These advantages produced efficient emission by **4-a** (Figures S20 and S21).

The photophysical properties of the $Eu^{3+}$ complexes were measured in dichloromethane ($CH_2Cl_2$) solutions (Figures S8 and S9, Table S14). The $\Phi_{f\text{-}f}$ and $\eta_{sens}$ values were still high ($\Phi_{f\text{-}f} \geq$ 61%, $\eta_{sens} \geq$ 0.84), which indicated that the present Eu(hfa) complexes with arsine ligands exhibited efficient emissions even in solutions. In particular, the relatively high $k_r$ and low $k_{nr}$ values of **4-a** were also observed in a solution, leading to the excellent $\Phi_{f\text{-}f}$ (72%). The overall PL intensity of $Eu^{3+}$ is defined as $I_{PL} = \Phi_{tot} \times \varepsilon$ ($\varepsilon$: molar extinction coefficient at the absorption maximum) (Table S17). The $I_{PL}$ value of **4-a** ($5.1 \times 10^4$ L/mol·cm) was much larger than that of **1-a** ($2.9 \times 10^3$ L/mol·cm). The relatively large π-system of ligand **4** made the main contribution to the large $\varepsilon$, resulting in the intensive emission (Figure S22).

We attempted to determine the deactivation pathways of the $Eu(hfa)_3$ complexes. The $T_1$ level of an $Eu^{3+}$ complex is highly dependent on the π-conjugated system of the antenna ligand (Figure 5a). Thus, the photophysical properties of the $Gd^{3+}$ complexes (**1b**, **2b**, **3b**, and **4b**), corresponding to the coordination structure of the $Eu^{3+}$ complexes, were investigated (Figure 5b and Table S16). Generally, in $Gd^{3+}$ complexes, the excited state ($^6P_{7/2}$) exists on the high-energy level. Hence, there is no energy transfer from the $T_1$ of the ligand to the $Eu^{3+}$ center.[12] This is why the $Gd^{3+}$ complex was suitable for the estimation of the $T_1$ level of the ligand in the corresponding $Ln^{3+}$ complex with a coordination structure similar to that of the $Gd^{3+}$ complex. From the vibrational Gaussian fitting curves in the PL spectra, the $T_1$ levels of **1-b**, **2-b**, **3-b**, and **4-b** were estimated to be 22300, 22400, 21500, and 21400 $cm^{-1}$, respectively (Figures 5c, 5d, and S14). The PL spectra of **1-b** and **2-b** were very similar

to that of $Gd(hfa)_3(H_2O)_2$, which indicated that their $T_1$ levels were derived from the hfa ligands. In contrast, the $T_1$ levels of **3-b** and **4-b** were from the arsine oxide ligands, judging from their PL spectra, which were different from that of $Gd(hfa)_3(H_2O)_2$. In the process of energy transfer, the $^5D_1$ (19000 $cm^{-1}$) and $^5D_2$ (21200 $cm^{-1}$) of the $Eu^{3+}$ were accessible from the $T_1$ levels of the ligands. The energy gap ($\Delta E(^3\pi\text{-}\pi^*\text{–}^5D_0)$) between the donor ($T_1$ of ligand) and acceptor ($^5D_0$ of $Eu^{3+}$: 17250 $cm^{-1}$) should be more than 2500 $cm^{-1}$ to avoid thermally activated back energy transfer (BET) according to Latva's semi-empirical rule; when $\Delta E(^3\pi\text{-}\pi^*\text{–}^5D_0)$ is less than 1850 $cm^{-1}$, a significant BET occurs.[13] Because the $\Delta E(^3\pi\text{-}\pi^*\text{–}^5D_0)$ values of all the $Eu^{3+}$ complexes were larger than 2500 $cm^{-1}$ (**1-a**: 5050 $cm^{-1}$, **2-a**: 5150 $cm^{-1}$, **3-a**: 4250 $cm^{-1}$, **4-a**: 4150 $cm^{-1}$), a BET was avoided, which was beneficial for efficient emission. This is why the $\eta_{sens}$ values of the $Eu^{3+}$ complexes were sufficiently high (0.80–0.85). Then, the influence of quenching by energy transfer to triplet oxygen ($^3O_2$), which generated singlet oxygen ($^1O_2$), was examined. The PL measurements were performed under an Ar atmosphere and in air (Table S15 and Figures S11–S13), and negligible differences were observed in the $\tau_{obs}$ and $\Phi_{f\text{-}f}$ values, which indicated that $k_{nr}$ was not affected by the measurement atmosphere. Therefore, no energy transfer to $^3O_2$ occurred in the present case.

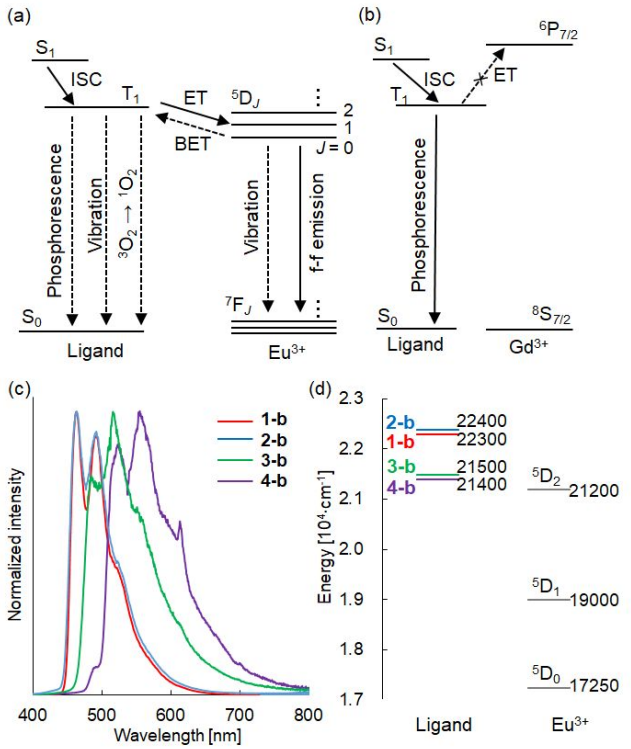


**Fig. 5** Jablonski diagram of (a) $Eu^{3+}$ and (b) $Gd^{3+}$ complexes in this work. Solid line: electron transitions responsible for fluorescence. Dashed line: electron transitions related to non-phosphorescence deactivation. (c) Emission spectra of **1-b**, **2-b**, **3-b**, and **4-b** in the solid state at 77 K on excitation at 335 nm. (d) $T_1$ levels estimated from the phosphorescence spectra of $Gd^{3+}$ complexes.

Finally, thermal stability of the luminescence was evaluated because the luminescence under high temperature is important in practical applications.[14] The variable-temperature PL (VT-PL) spectra were measured under $N_2$ atmosphere with heating from 300 to 500 K (Figures 6a-d and S18). It is notable that **4-a** showed emission even at 500 K, whereas the emissions of the others disappeared at 500 K. To confirm the luminescence at 500 K, the solid samples were heated on a hot plate at 500 K in air. The luminescence of **4-a** was visible by a naked eye, though those of the others were negligible (Figures 6e, S23, and S24). In addition, after cooling to 298 K, the samples of **1-a**, **2-a**, and **3-a**, which were originally colorless, turned brown, and the luminescence was significantly weakened. Conversely, the luminescence of **4-a** was recovered after cooling. These observations indicated that **4-a** has excellent durability against heating and is suitable for practical applications.

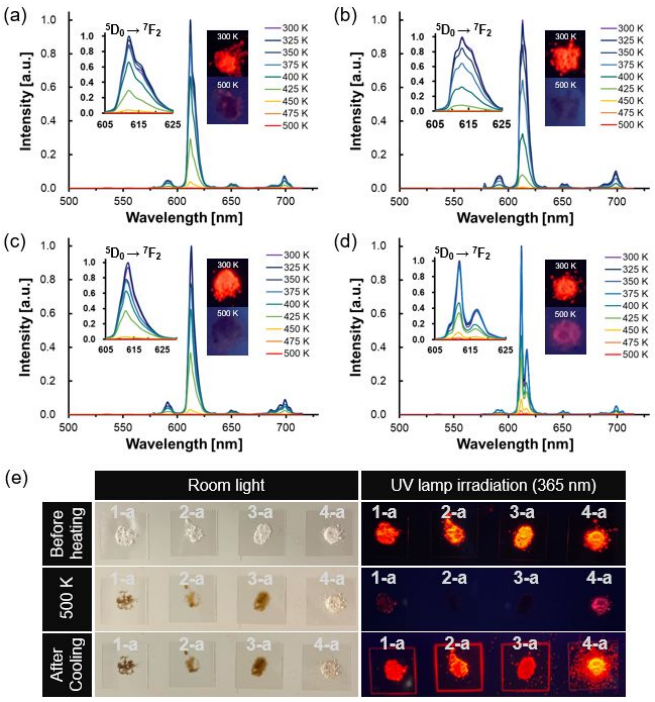


**Fig. 6** VT-PL spectra of (a) **1-a**, (b) **2-a**, (c) **3-a**, and (d) **4-a** excited at 365 nm. (e) Photographs of **1-a**, **2-a**, **3-a**, and **4-a** solid samples heated to 500 K under irradiation of room light and UV lamp (365 nm).

## Conclusion

$Eu^{3+}$ complexes with arsine oxide and hfa ligands were successfully synthesized. The hfa ligands were found to be more effective in restricting the non-radiative deactivation than the nitrate ligands, and the arsine oxide induced a greater electron dipole transition than the corresponding phosphine oxide. Consequently, an intense red emission was achieved, particularly with tri(1-naphtyl)arsine oxide, which produced a high quantum yield and enhanced the electron dipole transition. Notably, VT-PL measurments revealed that the $Eu^{3+}$ complex with tri(1-naphtyl)arsine oxide exhibited luminescence even at 500 K. This was the first study to examine the

correlation between the structures and photophysical properties of $Ln(hfa)_3$ complexes with arsine oxides. The results indicated that both hfa and arsine oxide hold promise for generating highly efficient emission. The insights gained from this study are expected to facilitate the further development of luminescent lanthanide complexes.

## Experimental

### Materials

Dichloromethane ($CH_2Cl_2$) and methanol (MeOH) were purchased from Nacalai Tesque, Inc. (Kyoto, Japan). *n*-Hexane, europium(III) acetate hydrate ($(CH_3COO)_3Eu{\cdot}nH_2O$), and gadolinium(III) acetate hydrate ($(CH_3COO)_3Gd{\cdot}nH_2O$) were purchased from Wako Pure Chemical Industry, Ltd. (Osaka, Japan). Hexafluoroacetylacetone (hfa) was purchased from Tokyo Kasei, Inc. (Tokyo, Japan). Triphenylarsine oxide (**1**),[15] triphenylphosphine oxide (**2**),[16] 9-phenyl-9-arsafluorene oxide (**3**),[7] tri(1-naphthyl)arsine oxide (**4**),[17] $Eu(hfa)_3(H_2O)_2$,[4] $Gd(hfa)_3(H_2O)_2$[4], $Eu^{3+}$-complex of **2** (**2-a**),[10] and $Gd^{3+}$-complex of **2** (**2-b**)[18] were synthesized according to literature procedures.

### Measurement

$^1H$ (400 MHz) and $^{13}C$ (100 MHz) NMR spectra were recorded on a Bruker AVANCE III 400 spectrometer. The samples were analyzed in $CDCl_3$ using $Me_4Si$ (TMS) as an internal standard. The following abbreviations are used: s, singlet; d, doublet; t, triplet; m, multiplet. High resolution mass spectra (HRMS) were obtained on a JEOL JMS-SX102A spectrometer. FT-IR spectra were obtained by using a JASCO FT/IR-4600 (Jasco, Tokyo, Japan) spectrometer. Thermogravimetric analysis (TGA) was performed using a Shimadzu TGA-50H thermogravimetric analyzer (Shimadzu, Kyoto, Japan) at a heating rate of 10 °C $min^{-1}$ under a $N_2$ flow. The UV–vis spectra were recorded on a Jasco spectrophotometer (V-670 KKN). Emission and phosphorescence spectra were obtained on an FP-8500 instrument (Jasco), and emission lifetimes were measured using Quantaurus-Tau (Hamamatsu Photonics). Variable temperature (VT) PL spectra were measured with a HORIBA JOBIN YVON Fluorolog–3 spectrofluorometer and an Oxford Optistat DN for temperature control. In terms of the phosphorescence measurement, the delay time was 55 ms. Absolute PL quantum yields ($\Phi$) were determined using a JASCO ILFC-847S instrument. In terms of the 4f–4f emission quantum yields ($\Phi_{f-f}$) and the radiative ($k_r$) and nonradiative ($k_{nr}$) rate constants were estimated (Table 1) using following eqs 2-6:

$$\tau_{rad} = \frac{1}{k_r} \quad (2)$$

$$\tau_{obs} = \frac{k_r}{k_r + k_{nr}} \quad (3)$$

$$\Phi_{f-f} = \frac{k_r}{k_r + k_{nr}} = \frac{\tau_{obs}}{\tau_{rad}} \quad (4)$$

$$k_r = A_{MD,0} n^3 \left(\frac{I_{tot}}{I_{MD}}\right) \quad (5)$$

$$k_{nr} = \frac{1}{\tau_{obs}} - \frac{1}{\tau_{rad}} \quad (6)$$

where $A_{MD,0}$ is the spontaneous emission probability for the $^5D_0 \rightarrow {}^7F_1$ transition in vacuo (14.65 $s^{-1}$), $n$ is the refractive index of the medium (refractive indices were 1.5 (solid state) and 1.426 ($CH_2Cl_2$ solution)), and ($I_{tot}/I_{MD}$) is the ratio of the total area of the corrected $Eu^{3+}$ emission spectrum to the area of the $^5D_0 \rightarrow {}^7F_1$ band.[19]

### X-ray crystallographic data for single crystalline products

The single crystal was mounted on a glass fiber. Intensity data were collected at 93 K or 293 K on a Rigaku XtaLAB mini with graphite-monochromated Mo Kα radiation. Readout was performed in 0.073 mm pixel mode. The data were collected to a maximum $2\vartheta$ value of 55.0°. Data were processed using CrysAlisPro.[20] An analytical numeric absorption correction[21] was applied. The data were corrected for Lorentz and polarization effects. The structure was solved by the ShelXT[22] and expanded using Fourier techniques. Non-hydrogen atoms were refined anisotropically. Hydrogen atoms were refined using the riding model. The final cycle of full-matrix least-squares refinement on $F_2$ was based on observed reflections and variable parameters. All calculations were performed using the Olex2[23] crystallographic software package except for refinement, which was performed using SHELXL2016.[24] Crystal data and more information on X-ray data collection are summarized in Tables S1-S4. Deposition Number 2291951 (**1-a**), 2291952 (**1-b**), 2291953 (**2-a**), 2291954 (**2-b**), 2291955 (**3-a**), 2291956 (**3-b**), 2291957 (**4-a**), and 2291958 (**4-b**) contain the supplementary crystallographic data for this paper. These data are provided free of charge by the joint Cambridge Crystallographic Data Centre and Fachinformationszentrum Karlsruhe Access Structures service.

### Computational detail

TD-DFT calculations to estimate dipole moment were carried out by B3LYP/6-31G+(d,p). NBO analysis for natural population analysis (NPA) was carried out by B3LYP/6-31G+(d,p).[25] These calculations were based on the geometries of **1**, **2**, **3**, and **4** within **1-a**, **2-a**, **3-a**, and **4-a**, respectively (Table S19). For all the calculation, Gaussian 16 code was employed. [26]

### Synthesis

*Note*: The lanthanide complexes were identified by single crystal X-ray structure analysis in addition to the following measurements.

*Eu-complex of **1** (**1-a**).* A MeOH solution (5.0 mL) of $Eu(hfa)_3(H_2O)_2$ (189 mg, 0.233 mmol) and **1** (151 mg, 0.468 mmol) was refluxed under stirring for 19 h. After the solvents were removed in *vacuo*, the residue was subjected to recrystallization from $CH_2Cl_2$ and hexane to obtain colorless crystal **1-a** (232 mg, 70 %). FT–IR (ATR): 1655 (C−O, s), 1088–1251 (C–F, s), 892 (As−O, s) $cm^{-1}$; HR–FAB–MASS: (m/z): calcd for $C_{46}H_{32}F_{12}O_6As_2Eu$ $[M–hfa]^+$, 1210.9646; found, 1210.9660.

*Eu-complex of **3** (**3-a**).* A MeOH solution (4.0 mL) of $Eu(hfa)_3(H_2O)_2$ (50.9 mg, 0.0629 mmol) and **3** (40.8 mg, 0.127 mmol) was refluxed under stirring for 13 h. After the solvents

were removed in *vacuo*, the residue was subjected to recrystallization from $CH_2Cl_2$ and hexane to obtain colorless crystal **3-a** (45.9 mg, 51 %). FT–IR (ATR): 1655 (C−O, s), 1094–1251 (C–F, s), 868 (As−O, s) $cm^{-1}$; HR–FAB–MASS: (m/z): calcd for $C_{46}H_{28}F_{12}O_6As_2Eu$ $[M–hfa]^+$, 1206.9333; found, 1206.9338.

*Eu-complex of **4** (**4-a**).* A MeOH solution (3.0 mL) of $Eu(hfa)_3(H_2O)_2$ (25.4 mg, 0.0314 mmol) and **4** (40.1 mg, 0.0626 mmol) was refluxed under stirring for 13 h. After the solvents were removed in *vacuo*, the residue was subjected to recrystallization from $CH_2Cl_2$, EtOH, and hexane to obtain colorless crystal **4-a** (37.9 mg, 36 %). FT–IR (ATR): 1656 (C−O, s), 1093–1251 (C–F, s), 864 (As−O, s) $cm^{-1}$; HR–FAB–MASS: (m/z): calcd for $C_{70}H_{44}F_{12}O_6As_2Eu$ $[M–hfa]^+$, 1511.0585; found, 1511.0601.

*Gd-complex of **1** (**1-b**).* A MeOH solution (3.0 mL) of $Gd(hfa)_3(H_2O)_2$ (50.8 mg, 0.0624 mmol) and **1** (40.6 mg, 0.126 mmol) was refluxed under stirring for 14 h. After the solvents were removed in *vacuo*, the residue was subjected to recrystallization from $CH_2Cl_2$ and hexane to obtain colorless crystal **1-b** (38.3 mg, 64 %). FT–IR (ATR): 1655 (C−O, s), 1087–1252 (C–F, s), 897 (As−O, s) $cm^{-1}$; HR–FAB–MASS: (m/z): calcd for $C_{46}H_{32}F_{12}O_6As_2Gd$ $[M–hfa]^+$, 1215.9675; found, 1215.9677.

*Gd-complex of **3** (**3-b**).* A MeOH solution (3.0 mL) of containing $Gd(hfa)_3(H_2O)_2$ (51.0 mg, 0.0626 mmol) and **3** (40.7 mg, 0.127 mmol) was refluxed under stirring for 27 h. After the solvents were removed in *vacuo*, the residue was subjected to recrystallization from $CH_2Cl_2$ and hexane to obtain colorless crystal **3-b** (49.6 mg, 57 %). FT–IR (ATR): 1654 (C−O, s), 1097–1252 (C–F, s), 880 (As−O, s) $cm^{-1}$; HR–FAB–MASS: (m/z): calcd for $C_{46}H_{28}F_{12}O_6As_2Gd$ $[M–hfa]^+$,1211.9362; found, 1211.9371.

*Gd-complex of **4** (**4-b**).* A MeOH solution (4.0 mL) of containing $Gd(hfa)_3(H_2O)_2$ (25.6 mg, 0.0314 mmol) and **4** (40.5 mg, 0.0632 mmol) was refluxed under stirring for 18 h. After the solvents were removed in *vacuo*, the residue was subjected to recrystallization from $CH_2Cl_2$ and hexane to obtain colorless crystal **4-b** (45.3 mg, 70 %). FT–IR (ATR): 1657 (C−O, s), 1095–1251 (C–F, s), 881 (As−O, s) $cm^{-1}$; HR–FAB–MASS: (m/z): calcd for $C_{70}H_{44}F_{12}O_6As_2Gd$ $[M–hfa]^+$, 1516.0614; found, 1516.0617.

## Author Contributions

H. Shimoji: Synthesis, structural analysis, photophysical analysis, data curation, writing – original draft; T. Fujii: Synthesis, structural analysis, photophysical analysis, data curation, writing – original draft; A. Sumida: Structural analysis, data curation, writing – original draft; Y. Kitagawa: Structural analysis, photophysical analysis, data curation, writing – original draft; Y. Hasegawa: Structural analysis, photophysical analysis, data curation, writing – original draft; H. Imoto: conceptualization, investigation, data curation, writing – original draft, writing – review and editing, funding acquisition project administration, supervision; K. Naka: conceptualization, investigation, writing – review and editing, funding acquisition, project administration, supervision

## Conflicts of interest

There are no conflicts to declare.

## Acknowledgements

This work was supported by JST FOREST Program (Grant Number JPMJFR221K) to HI.

## Notes and references

1 a) Y. Hasegawa, Y. Kitagawa and T. Nakanishi, *NPG Asia Materials.*, 2018, **10**, 52–70; b) S. E. Bodman and S. J. Butler, *Chem. Sci.*, 2021, **12**, 2716–2734; c) Y. Kitagawa, M. Tsurui and Y. Hasegawa, *RSC Adv*. 2022, **12**, 810–821; d) K. Kuriki and Y. Koike, *Chem. Rev.*, 2002, **102**, 2347–2356; e) J. -C. G. Bünzli, *Chem. Rev.*, 2010, **110**, 2729–2755; f) K. Binnemans, *Chem. Rev.*, 2009, **109**, 4283–4374; g) M. Hasegawa and H. Ohmagari, *Chem. Lett.*, 2020, **49**, 845–854; h) M. Y. Berezin and S. Achilefu, *Chem. Rev.*, 2010, **110**, 2641–2684; i) J. Kido and Y. Okamoto, *Chem. Rev.*, 2002, **102**, 2357–2388; j) H. Dong, S. -R. Du, X. -Y. Zheng, G. -M. Lyu, L. -D. Sun, L. -D. Li, P. -Z. Zhang, C. Zhang and C. -H. Yan, *Chem. Rev.*, 2015, **115**, 10725–10815.

2 a) M. W. Mara, D. S. Tatum, A. -M. March, G. Doumy, E. G. Moore and K. N. Raymond, *J. Am. Chem. Soc.*, 2019, **141**, 11071–11081; b) S. Miyazaki, K. Miyata, H. Sakamoto, F. Suzue, Y. Kitagawa, Y. Hasegawa and K. Onda, *J. Phys. Chem. A*, 2020, **124**, 6601–6606; c) G. -Q. Jin, Y. Ning, J. -X. Geng, Z. -F. Jiang, Y. Wang and J. -L. Zhang, *Inorg. Chem. Front.*, 2020, **7**, 289–299; d) P. A. Tanner, W. Thor, Y. Zhang and K. -L. Wong, *J. Phys. Chem. A*, 2022, **126**, 7418–7431; e) A. K. R. Junker, L. R. Hill, A. L. Thompson, S. Faulkner and T. J. Sørensen, *Dalton Trans.*, 2018, **47**, 4794–4803; f) S. I. Klink, G. A. Hebbink, L. Grave, P. B. O. Alink, F. C. J. M. v. Veggel and M. H. V. Werts, *J. Phys. Chem*. *A*, 2002, **106**, 3681–3689.

3 a) K. Miyata, T. Nakagawa, R. Kawakami, Y. Kita, K. Sugimoto, T. Nakashima, T. Harada, T. Kawai and Y. Hasegawa, *Chem. Eur. J.*, 2011, **17**, 521–528; b) N. M. Shavaleev, S. V. Eliseeva, R. Scopelliti and J. -C. G. Bünzli, *Inorg. Chem.*, 2015, **54**, 9166–9173; c) K. Yanagisawa, Y. Kitagawa, T. Nakanishi, T. Akama, M. Kobayashi, T. Seki, K. Fushimi, H. Ito, T. Taketsugu and Y. Hasegawa, *Eur. J. Inorg. Chem.*, 2017, **32**, 3843–3848.

4 a) T. Koizuka, K. Yanagizawa, Y. Hirai, Y. Kitagawa, T. Nakanishi, K. Fushimi and Y. Hasegawa, *Inorg. Chem.*, 2018, **57**, 7097–7103; b) Y. Hirai, T. Nakanishi, Y. Kitagawa, K. Fushimi, T. Seki, H. Ito and Y. Hasegawa, *Angew. Chem. Int. Ed.*, 2016, **55**, 12059–12062; c) Y. Hasegawa, M. Yamamuro, Y. Wada, N. Kanehisa, Y. Kai and S. Yanagida, *J. Phys. Chem. A*, 2003, **107**, 1697–1702.

5 a) H. Xu, L. -H. Wang, X. -H. Zhu, K. Yin, G. -Y. Zhong, X. -Y. Hou and W. Huang, *J. Phys. Chem. B*, 2006, **110**, 3023–3029; b) C. Ebenezer and R. V. Solomon, *New J. Chem.*, 2022, **46**, 5761; c) F. J. Sainz-Gonzalo, M. Casimiro, C. Popovici, A. Rodríguez-Diéguez, J. F. Fernández-Sánchez, I. Fernández, F. López-Ortiz and A. Fernández-Gutiérrez, *Dalton Trans.*, 2012, **41**, 6735–6748; d) K. Yanagisawa, T. Nakanishi, Y. Kitagawa, T. Seki, T. Akama, M. Kobayashi, T. Taketsugu, H. Ito, K. Fushimi and Y. Hasegawa, *Eur. J. Inorg. Chem.*, 2015, **28**, 4769–4774; e) A. S. Silva, N. D. Lima, A. Simas and S. C. Gonçalves, *ACS Omega*, 2017, **2**, 6786–6794.

6 T. Fujii, Y. Kitagawa, Y. Hasegawa, H. Imoto and K. Naka, *Inorg. Chem.*, 2021, **60**, 8605–8612.

7 T. Fujii, Y. Kitagawa, Y. Hasegawa, H. Imoto and K. Naka, *Inorg. Chem.*, 2022, **61**, 17662–17672.

8 T. Koizuka, M. Yamamoto, Y. Kitagawa, T. Nakanishi, K. Fushimi and Y. Hasegawa, *Bull. Chem. Soc. Jpn.*, 2017, **90**, 1287–1292.
9 a) Y. Kitagawa, F. Suzue, T. Nakanishi, K. Fushimi and Y. Hasegawa, *Dalton Trans.*, 2018, **47**, 7327–7332; b) Y. A. Bryleva, V. Y. Komarov, L. A. Glinskaya, A. V. Artem'ev, M. P. Davydova, M. I. Rakhmanova and D. G. Samsonenko, *New J. Chem.*, 2023, **47**, 10446–10454; c) O. Moudam, B. C. Rowan, M. Alamiry, P. Richardson, B. S. Richards, A. C. Jones and N. Robertson, *Chem. Commun.*, 2009, **43**, 6649–6651; d) K. Miyata, Y. Hasegawa, Y. Kuromochi, T. Nakagawa, T. Yokoo and T. Kawai, *Eur. J. Inorg. Chem.*, 2009, **32**, 4777–4785; e) M. Pietraszkiewicz, M. Maciejczyk, I. D. W. Samuel and S. Zhang, *J. Mater. Chem. C*, 2013, **1**, 8028–8032.
10 Y. Hasegawa, T. Ohkubo, T. Nakanishi, A. Kobayashi, M. Kato, T. Seki, H. Ito and K. Fushimi, *Eur. J. Inorg. Chem.*, 2013, **34**, 5911–5918.
11 D. Casanova, M. Llunell, P. Alemany and S. Alvarez, *Chem. Eur. J.*, 2005, **11**, 1479–1494.
12 a) G. Yu, Y. Xing, F. Chen, R. Han, J. Wang, Z. Bian, L. Fu, Z. Liu, X. Ai, J. Zhang and C. Huang, *ChemPlusChem*, 2013, **78**, 852–859; b) A. R. Ramya, D. Sharma, S. Natarajan and M. L. Reddy, *Inorg. Chem.*, 2012, **51**, 8818–8826; c) H. Liu, Y. Liu, Y. Meng, X. Shi, J. Sun, L. Zhao, D. Chen, H. Hao, D. Li, J. Dou and J. Han, *RSC Adv.*, 2020, **10**, 32232–32240; d) W. Jiang, B. Lou, J. Wang, H. Lv, Z. Bian and C. Huang, *Dalton Trans*., 2011, **40**, 11410–11418; e) H. Dong, L. -D. Sun and C. -H. Yan, *Chem. Soc. Rev.*, 2015, **44**, 1608–1634.
13 M. Latva, H. Takalo, V. -M, Mukkala, C. Matachescu, J. C. Rodríguez-Ubis and J. Kankare, *J. Lumin.*, 1997, **75**, 149–169.
14 a) M. Gon, S. Saotome, K. Tanaka and Y. Chujo, *ACS appl. Mater. Interfaces*., 2021, **13**, 12483–12490. b) M Y. Wong and E. Zysman-Colman, *Adv. Mater.* 2017, **29**, 1605444. c) S. Scholz, D. Kondakov, B. Lüssem and K. Leo, *Chem*. *Rev*., 2015, **115**, 8449–8503.
15 M. Donath, M. Bodensteiner and J. J. Weigand, *Chem. Eur. J.*, 2014, **20**, 17306–17310.
16 C. -S. Wang, P. H. Dixneuf and J. -F. Soulé, *ChemCatChem*, 2017, **9**, 3117–3120.
17 H. Kihara, H. Imoto and K. Naka, *Asian J. Org. Chem.*, 2021, **10**, 2682–2689.
18 M. Yamamoto, Y. Kitagawa, T. Nakanishi, K. Fushimi and Y. Hasegawa, *Chem. Eur. J.*, 2018, **24**, 17719–17726.
19 M. H. V. Werts, R. T. F. Jukes and J. W. Verhoeven, *Phys. Chem. Chem. Phys.*, 2002, **4**, 1542–1548.
20 CrysAlisPro Software System, Rigaku Oxford Diffraction, 2020.
21 Analytical numerical absorption correction multi-faceted crystal model: R. C. Clark and J. S. Reid, *Acta Crystallogr.*, *Sect. A: Found. Crystallogr.* 1995, **A51**, 887-897.
22 G. M. Sheldrick, *Acta Crystallogr., Sect. C: Struct. Chem.*, 2015, **A71**, 3-8.
23 O. V. Dolomanov, L. J. Bourhis, R. J. Gildea, J. A. K. Howard and H. J. Puschmann, Olex2, *J. Appl. Crystallogr.*, 2009, **42**, 339-341.
24 G. M. Sheldrick SHELXL2016, *Acta Crystallogr., Sect. C: Struct. Chem.*, 2015, **C71**, 3-8.
25 A. E.; Curtiss and L. A.; Weinhold, F. Intermolecular interactions from a natural bond orbital, donor-acceptor viewpoint. *Chem. Rev.*, 1988, **88**, 899–926.
26 Gaussian 16, Revision B.01, M. J. Frisch, G. W. Trucks, H. B. Schlegel, G. E. Scuseria, M. A. Robb, J. R. Cheeseman, G. Scalmani, V. Barone, G. A. Petersson, H. Nakatsuji, X. Li, M. Caricato, A. V. Marenich, J. Bloino, B. G. Janesko, R. Gomperts, B. Mennucci, H. P. Hratchian, J. V. Ortiz, A. F. Izmaylov, J. L. Sonnenberg, D. Williams-Young, F. Ding, F. Lipparini, F. Egidi, J. Goings, B. Peng, A. Petrone, T. Henderson, D. Ranasinghe, V. G. Zakrzewski, J. Gao, N. Rega, G. Zheng, W. Liang, M. Hada, M. Ehara, K. Toyota, R. Fukuda, J. Hasegawa, M. Ishida, T. Nakajima, Y. Honda, O. Kitao, H. Nakai, T. Vreven, K. Throssell, J. A. Montgomery, Jr., J. E. Peralta, F. Ogliaro, M. J. Bearpark, J. J. Heyd, E. N. Brothers, K. N. Kudin, V. N. Staroverov, T. A. Keith, R. Kobayashi, J. Normand, K. Raghavachari, A. P. Rendell, J. C. Burant, S. S. Iyengar, J. Tomasi, M. Cossi, J. M. Millam, M. Klene, C. Adamo, R. Cammi, J. W. Ochterski, R. L. Marin, K. Morokuma, O. Farkas, J. B. Foresman and D. J. Fox, Gaussian, Inc., Wallingford CT, 2016.

 